2012

A Comprehensive Search for Stable Pt–Pd Nanoalloy Configurations and Their Use as Tunable Catalysts

Teck L. Tan
Agency for Science, Technology and Research

Lin-Lin Wang
Ames Laboratory, llw@ameslab.gov

Duane D. Johnson
Iowa State University, ddj@iastate.edu

Kewu Bai
Agency for Science, Technology and Research

A Comprehensive Search for Stable Pt–Pd Nanoalloy Configurations and Their Use as Tunable Catalysts

Abstract

Using density-functional theory, we predict stable alloy configurations (ground states) for a 1 nm Pt–Pd cuboctahedral nanoparticle across the entire composition range and demonstrate their use as tunable alloy catalysts via hydrogen-adsorption studies. Unlike previous works, we use simulated annealing with a cluster expansion Hamiltonian to perform a rapid and comprehensive search that encompasses both high and low-symmetry configurations. The ground states show Pt(core)–Pd(shell) type configurations across all compositions but with specific Pd patterns. For catalysis studies at room temperatures, the ground states are more realistic structural models than the commonly assumed random alloy configurations. Using the ground states, we reveal that the hydrogen adsorption energy increases (decreases) monotonically with at. % Pt for the {111} hollow ({100} bridge) adsorption site. Such trends are useful for designing tunable Pd–Pt nanocatalysts for the hydrogen evolution reaction.

Keywords

Materials Science and Engineering, First-principles, Cluster expansion, Nanoalloy, Hydrogen adsorption, Od, Pt, Hydrogen evolution, Catalysis

Disciplines

Condensed Matter Physics | Materials Science and Engineering | Physical Chemistry

Comments

Reprinted with permission from *Nano Lett.*, **2012**, 12(9), pp. 4875–4880, doi:10.1021/nl302405k.

NANO LETTERS

Letter

pubs.acs.org/NanoLett

A Comprehensive Search for Stable Pt−Pd Nanoalloy Configurations and Their Use as Tunable Catalysts

Teck L. Tan,*[,†] Lin-Lin Wang,[‡] Duane D. Johnson,[‡,§] and Kewu Bai[†]

[†]Institute of High Performance Computing, Agency for Science, Technology and Research, Singapore 138632, Singapore

[‡]Ames Laboratory, U.S. Department of Energy, Ames, Iowa 50011-3020, United States

[§]Department of Materials Science and Engineering, Iowa State University, Ames, Iowa 50011, United States

Supporting Information

ABSTRACT: Using density-functional theory, we predict stable alloy configurations (ground states) for a 1 nm Pt−Pd cuboctahedral nanoparticle across the entire composition range and demonstrate their use as tunable alloy catalysts via hydrogen-adsorption studies. Unlike previous works, we use simulated annealing with a cluster expansion Hamiltonian to perform a rapid and comprehensive search that encompasses both high and low-symmetry configurations. The ground states show Pt(core)−Pd(shell) type configurations across all compositions but with specific Pd patterns. For catalysis studies at room temperatures, the ground states are more realistic structural models than the commonly assumed random alloy configurations. Using the ground states, we reveal that the hydrogen adsorption energy increases (decreases) monotonically with at. % Pt for the {111} hollow ({100} bridge) adsorption site. Such trends are useful for designing tunable Pd−Pt nanocatalysts for the hydrogen evolution reaction.

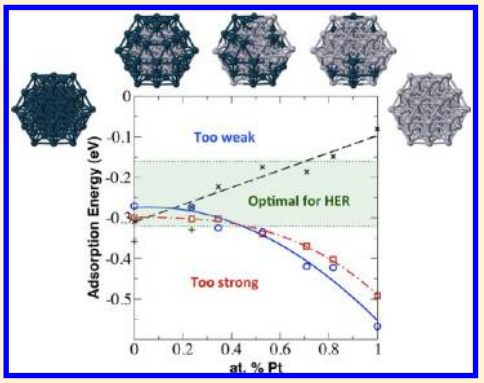

KEYWORDS: *First-principles, cluster expansion, nanoalloy, hydrogen adsorption, Pd, Pt, hydrogen evolution reaction, catalysis*

Bimetallic nanoparticles (nanoalloys) have found use in a number of applications, including catalysis.[1] Although the properties of nanoalloy are highly affected by the configurations (atomic arrangements) that exist, it is difficult to experimentally determine the exact chemical ordering,[2,3] which differs from the bulk phase as well. Bulk alloys that mix may not do so in nanoalloys because differences in surface energies could drive the formation of core−shell (segregated) configurations.[4] Hence, many computational studies are focusing on structural predictions of nanoalloys. For Pt−Pd nanoalloy, structural searches via empirical potentials,[5,6] tight-binding,[7−9] and more recently via (first-principles) density functional theory (DFT) calculations[10] have been done. As empirical potentials are sensitive to parametrization, first-principles calculations are preferred when highly accurate structural energies are required. However, the latter is computationally expensive, and a direct search for low-energy configurations on a fixed shape nanoalloy quickly becomes intractable with increasing particle size; an n-atom bimetallic particle would require 2^n evaluations. To reduce the search space, one may artificially group atomic sites with equivalent symmetry[10] and restrict the search to only a few symmetry-preserving stoichiometry. Such a search would miss energetically stable configurations of low symmetry.

To conduct a comprehensive search for stable nanoalloy configurations, we use the cluster expansion (CE) method[11]—the search is not restricted to high-symmetry configurations. A cluster Hamiltonian is constructed from a set of DFT energies of various configurations and its success is built upon the fact that the strongest cluster interactions are usually short ranged in metal alloys;[12−14] one only needs a finite number of cluster interactions to reproduce accurately the configuration energies. Coupled with Monte Carlo simulated annealing, the CE enables a rapid but extensive search over ∼10^6 configurations for low-energy states. We show that, for a 1 nm particle, the ground states exhibit Pt(core)-Pd(shell) configurations across all compositions with specific Pd patterns which may not be of high symmetry.

An alloy-composition map detailing site-specific occupation[15] is of great use for designing nanoalloy catalysts as specific chemical ordering in alloy catalysts strongly impacts catalytic behavior via ligand[16] and ensemble[17] effects. In the absence of such knowledge, catalytic models are often built using random solutions.[18,19] Comparatively, the ground states are more realistic models for catalysts operating under room conditions, as they are energetically more stable and agree better with structural data from experiments (see the Supporting Information). Using hydrogen atom as a probe, we perform a systematic study of the hydrogen adsorption energies (E_{ads}) at specific sites using the predicted ground states at different at. % Pt. This leads to an interesting discovery—E_{ads} of different nanoparticle (NP) facets exhibit opposite trends. Using the

Received: June 28, 2012
Revised: August 9, 2012
Published: August 15, 2012

adsorption energies, we further speculate how the addition of Pd to Pt would improve the catalytic activity for the hydrogen evolution reaction (HER).[20,21] Our calculations show that the activity in 1 nm-size Pt NPs is lower than that of Pt surface due to size effect,[22,23] and the addition of Pd improves the catalytic activity by appropriately tuning E_{ads}. Although one ideally desires a temperature−composition−coverage phase diagram, where coverage effects may potentially alter local atomic arrangements, limited H-adsorption cannot change the trends predicted here, as discussed.

Computational Model and Approach. For FCC metals or alloys, commonly observed FCC-derived NP shapes include the truncated octahedron and cuboctahedron[1,24] and possibly the icosahedron in the free-standing case. For ∼1 nm size Pt NPs, although amorphous clusters[25] are preferred, H-adsorption has been shown to stabilize the cuboctahedron NP by removing the shear instability of {100} facets.[26] In addition, cuboctahedral Pt−Pd nanoalloys with diameters between 1 and 5 nm (with Pd segregated to the outer shell) have been observed experimentally for particles prepared via colloidal synthesis[2,3,27] and via laser vaporization techniques.[28,29]

As such, we use a 55-atom cuboctahedron (∼1 nm in diameter) as the model for the nanoalloy with each atomic site being occupied by either a Pd or Pt atom. Energies of nanoalloy configurations are computed using density functional theory (DFT)[30,31] to obtain reliable relative energies. DFT calculations were done using Vienna ab initio simulation package (VASP)[32,33] within a projected augmented wave (PAW) basis,[34] based on the generalized-gradient approximation (GGA) using the PW91[35] exchange-correlation functional (revised PBE functional[36] for H adsorption).

Using calculated DFT formation energies as the learning set, we construct a CE Hamiltonian for the Pd−Pt cuboctahedron. The Hamiltonian is a linear expansion in terms of atomistic cluster correlations, and with appropriate truncation, one only needs a small set of clusters to accurately reproduce the alloy configuration DFT energies. Because only atomistic interactions are present, the CE enables rapid evaluation of millions of configurations, sufficient to address reliably alloy thermodynamics, and has been applied extensively to bulk alloys[11,12,37−50] and recently nanoalloys.[15,51,52] An iterative procedure combining CE with simulated annealing is used for searching low-energy configurations where newly predicted stable configurations are verified by DFT; a feedback procedure is used where the new DFT energies are added to the learning set for constructing the next CE. Additional details are furnished in the Supporting Information.

Results and Discussion. *Pd−Pt Nanoalloy Ground States.* The iterative search results in a formation energy database of 340 configurations which are shown in Figure 1. The formation energy (from DFT) of each configuration, $\vec{\sigma}$, is defined as

$$E_f(\vec{\sigma}) = \frac{1}{55}\{E^{DFT}(\vec{\sigma}) - x_{Pt}E^{DFT}(Pt) - x_{Pd}E^{DFT}(Pd)\} \quad (1)$$

with x_{Pt} and x_{Pd} the Pt and Pd compositions, respectively, and they satisfy the sum rule, $x_{Pt} + x_{Pd} = 1$. Most initial ("guessed") configurations, some of which are of high symmetry, have high E_f as they are generated without a priori knowing the low-energy states. This shows that a restricted search over high symmetry configurations[10] is insufficient for identifying ground states. The CE in tandem with simulated annealing directs the search toward low-energy configurations; a high proportion of low-energy configurations are obtained in subsequent iterations. A lowest-energy hull is constructed, and it serves as the lower energy bound of the nanoalloy configurational energies. Configurations on the hull are ground states. States close to the hull are relatively more stable (low-energy excitations of the ground states) and are thus more likely to be observed in experiments at low temperatures. Formation energies of random alloy solutions are calculated using the CE Hamiltonian (see the Supporting Information), and the energy differences between the ground states and their corresponding random alloy solutions are a measure of their relative stability.

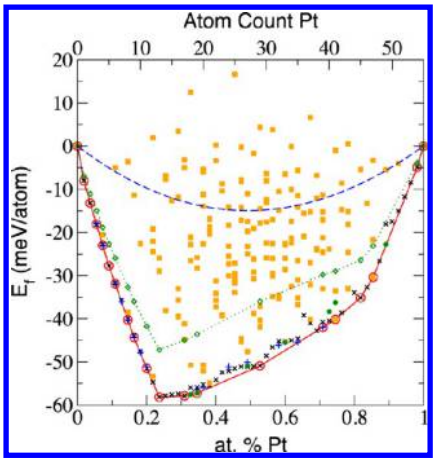

Figure 1. DFT formation energies of Pd−Pt nanoalloy configurations versus at. % Pt. Energies are bounded from below by a ground state hull (red line) that connects ground state energies (circles). DFT energies from each search iteration are labeled: 1st (filled squares), 2nd (×), 3rd (+), and 4th (filled circles). Also shown are the CE formation energies of the random solutions (dashed line) and energy differences (diamonds) between each ground state and its corresponding random solution at fixed stoichiometry, i.e., NP ordering energy.

We illustrate in Figure 2 selected ground states and near-ground states, showing site-specific occupation at different compositions. Importantly, the ground states exhibit Pt(core)−Pd(shell) properties across all compositions. This implies that Pt(core)−Pd(shell) nanoalloys (of ca. 1 nm) are energetically favored and indeed, the perfect core−shell structure, GS_{13}, has the lowest formation energy. The preference for Pt in the core can be attributed to its higher cohesive energy than Pd while having almost the same atomic radius.[4]

For Pt-rich compositions, one observes that the initial preferred segregation site for Pd is at the surface edge. These sites are populated with Pd (see GS_{47-54}) on two of the {100} facets before face-center sites are populated ($GS_{41,45}$). At Pd-rich compositions, Pt first occupies the central core site (GS_1) followed by the second inner shell (GS_{2-13}), and the formation energy decreases monotonically with each addition of Pt, clearly showing Pt's preference for core sites. When Pt atoms are added beyond GS_{13}, Pt starts to occupy the surface edge sites (GS_{14-19}), and the formation energy increases.

Segregation Profile Versus (100) Semi-Infinite Surface. The 55-atom cuboctahedron consists of mainly {100} facets. To show the effect of nanosize on alloy segregation, we compare the nanoalloy ground states with those obtained from a (100) semi-infinite surface modeled as a four-layer slab (see the Supporting Information). As shown in Figure 3, segregation of

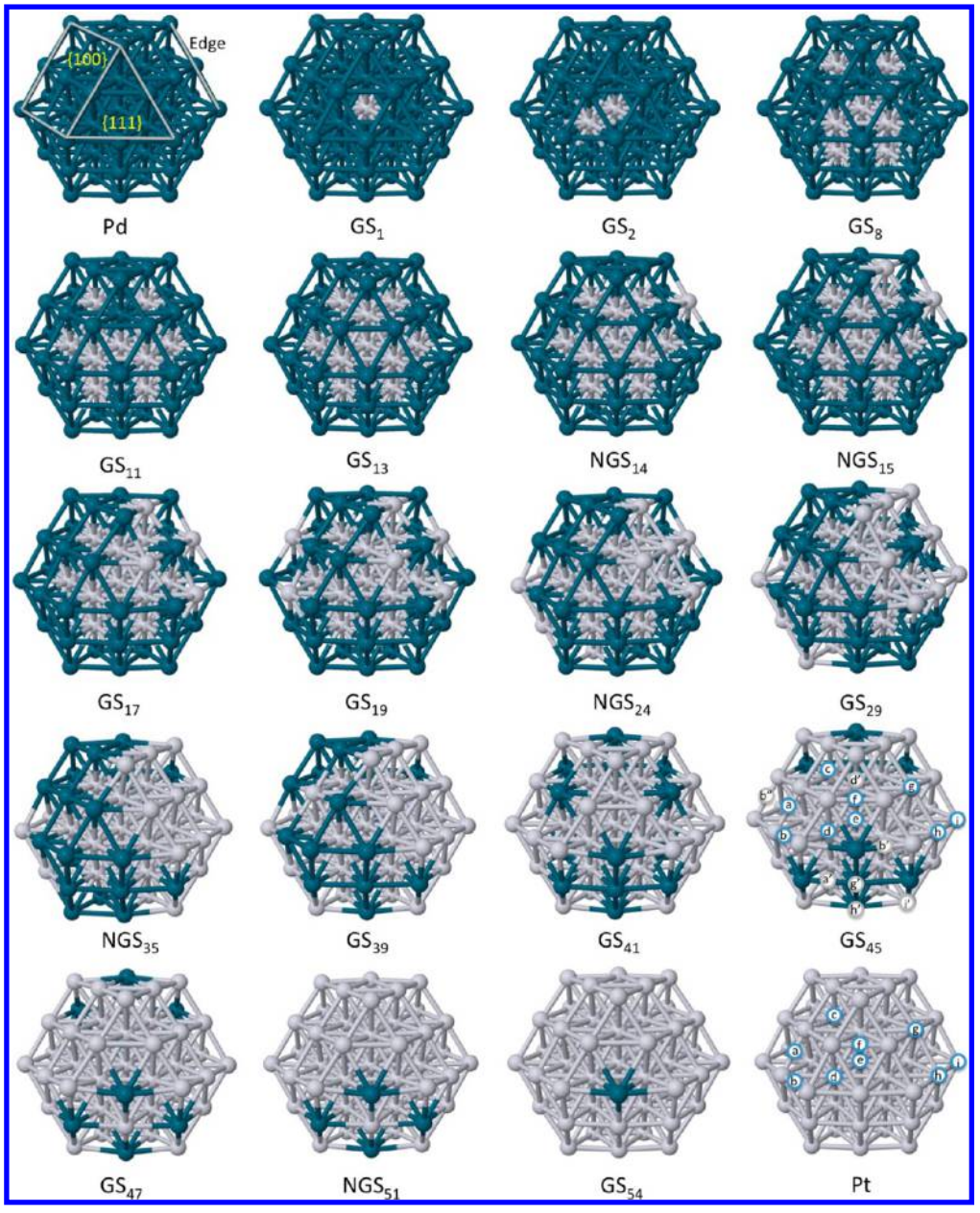

Figure 2. Selected ground states (GS_n) and near ground state (NGS_n) configurations for the Pd−Pt 55-atom cuboctahedron, where n is the number of Pt (gray) atoms, consisting of 8 {111} facets, 6 {100} facets, and 24 edges. The perfect core−shell structure, GS_{13}, has all 13 (42) core (shell) atomic sites occupied by Pt (Pd). For high-symmetry configurations (Pd, Pt, GS_1, and GS_{13}), the symmetry-distinct adsorption sites are illustrated using a Pt cluster, with {111} hollow sites (d and e), {100} hollow site (c), bridge sites (a, b, and f), and atop sites (g, h, and i). Lower-symmetry configurations such as GS_{45} contain additional unique adsorption sites.

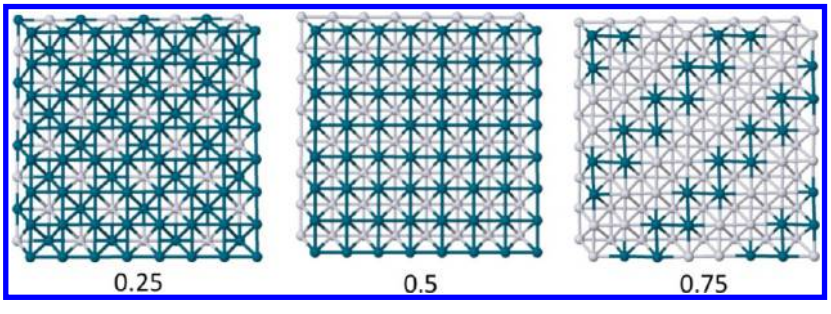

Figure 3. Selected ground states for the (100) Pd−Pt semi-infinite surface. Exchange of atoms is allowed for the top two layers, the bottom two layers (not shown) are occupied by Pt (see the Supporting Information). The configurations are labeled according to at. % Pt of the top two layers.

Table 1. Single H-Adsorption Energies (eV) on Various Sites for Pure Pt and Pd Surfaces and Selected Nanoalloys Calculated via DFT Using a Revised PBE Functional[a,b]

	hollow (fcc)	hollow (hcp)	hollow (square)	bridge			atop	
Pd (111)	−0.38	−0.34	N.A.	U			0.12	
Pd (100)	N.A.	N.A.	−0.33	−0.32			0.10	
Pd (nano)	−0.41 (e)	−0.42 (d)	−0.22 (c)	−0.26 (a)	U (b)	0.12 (g)	U (h)	0.18 (i)
Pt (111)	−0.32	−0.27	N.A.	U			−0.32	
Pt (100)	N.A.	N.A.	−0.09	−0.46			−0.31	
Pt (nano)	−0.15 (e)	−0.21 (d)	U (c)	−0.60 (a)	−0.44 (b)	−0.58 (g)	−0.44 (h)	−0.46 (i)
GS_{13}	−0.36 (e)	−0.37 (d)	−0.30 (c)	−0.25 (a)	−0.30 (b)	0.14 (g)	U (h)	0.18 (i)
GS_{45}	−0.23 (e)	−0.19 (d′)	U (c)	−0.50 (a)	−0.50 (b)	−0.50 (g)	−0.45 (h)	−0.50 (i′)
		U (d)		−0.45 (a′)	−0.37 (b″)	U (g′)	0.15 (h′)	−0.34 (i)
					−0.37 (b′)			

[a]For NPs, adsorption energies are followed by location indices shown in Figure 2. [b]Sites labeled "U" are unstable, and the H relaxes to an adjacent stable site of lower E_{ads}.

Pd (Pt) to the surface (subsurface) layers is also preferred. The ground state at x_{Pt} = 0.5, whose top (subsurface) layer is fully occupied by Pd (Pt), has the lowest formation energy (see Figure S3). The specific ordering pattern on the (100) surface, however, differs. In particular, Pd atoms exhibit a zigzag chain at x_{Pt} = 0.75 (Figure 3) and a dimer arrangement at higher Pt concentration of x_{Pt} = 0.875 (Figure S4), which are not observed in the nanoalloy case.

Nanoalloy Ground States Versus Random Alloys. Here, we justify the use of Pt(core)−Pd(shell) ground states (rather than random alloy states[19]) as catalytic models at room temperatures. From Figure 1, the energy of the perfect core−shell structure (GS_{13}) is 47 meV below that of the random alloy (ordering energy). As an estimate, observations of random states will become significant around 550 K at nearby compositions. Likewise, observations will be core−shell like between 0.1 < x_{Pt} < 0.85 at room temperatures (300 K), since the ground states are at least 26 meV more stable than random solutions in this range. Furthermore, the nearest-neighbor coordination numbers of the core−shell ground states are closer to experimental values than those obtained for random solutions (see Table S3).

Hydrogen Adsorption on Surfaces versus Nanoparticles. Before showing how Pd−Pt compositions affect hydrogen adsorption, we do a systematic evaluation of H adsorption on Pt and Pd cuboctahedron. In addition to their common occurrence in experiments, the cuboctahedron structure of Pt is also stabilized by adsorption of atomic H.[26] Adsorption energies are calculated via

$$E_{ads} = E_{M-mH} - E_M - \frac{m}{2}E_{H_2} \quad (2)$$

E_{M-mH} is the DFT energy of the nanocluster (or surface) with m adsorbed H atoms; E_M and E_{H_2} are the DFT energies of the bare nanocluster (or surface) and H_2 molecule. A more negative E_{ads} implies stronger adsorption.

Table 1 compares the adsorption of a single H atom (n = 1) on various NP adsorption sites. To elucidate the size effect, we compare the results with those from semi-infinite surfaces. The H coverage on the NP corresponds to 1/42 monolayer (ML), while that of the surfaces corresponds to a 0.25 ML; E_{ads} of the surface may be lowered by ca. 0.03 eV when the results are extrapolated to 1/42 ML.[53]

In general, H binds more strongly to Pd (Pt) on {111} ({100}) surfaces/facets. For Pt NP, adsorption at {100} bridge sites is most energetically favored, while that of {111} hollow site (hcp and fcc) is least favored. In contrast, a Pd NP shows stronger adsorption on {111} hollow sites than on the {100} bridge sites; adsorption on atop sites is highly unfavorable. Surfaces and NPs of the same metal display similar preferences for adsorption facets and sites, although the adsorption energies are altered due to the size effect. Interestingly, different facets on Pd and Pt are impacted differently. Adsorption strength on Pt NP {100} bridge site is enhanced over that of the (100) surface, while adsorption on {111} hollow sites is weakened compared to (111) surface. The reverse effect is seen for Pd, where adsorption on NP {111} hollow ({100} bridge) site is stronger (weaker) than those of semi-infinite surfaces.

H-Adsorption on Nanoalloy Ground States. Table 1 clearly shows that Pt NP adsorbs H more strongly (weakly) at bridge ({111} hollow) sites than Pd NP. Similar systematic evaluations are also shown for GS_{13} and GS_{45}, and in most cases, the adsorption energies lie between that of Pd and Pt cases. As a simple indicator of how alloying affects adsorption properties,[19] we calculate the mean E_{ads} of multiple H atoms adsorbed symmetrically on each facet for each unique adsorption site of interest in the selected ground states; for example, we adsorb one H atom on one of the bridge sites "a" on all six {100} facets (see Figure S6 of the Supporting Information). Mean adsorption energies are obtained using (2). The results in Figure 4 show that the adsorption energies on bridge sites and {111} hollow sites follow opposing trends. Bridge sites are most stable for compositions above ca. 15% Pt, while {111} hollow sites are most stable below 15% Pt. At Pt-rich compositions, adsorption energies at bridge sites are lower by ca. 0.4 eV compared to hollow sites, and this energy difference changes in a quadratic manner with composition. At Pd-rich compositions, {111} hollow sites are more stable by ca. 0.1 eV (compared to bridge sites), and the energy difference changes linearly with composition. This implies that adsorption characteristics are more sensitive to composition changes for Pt-rich alloys. The continuous change in adsorption energies demonstrates the possibility of tuning catalytic properties via alloying.

H-Adsorption Effect on Segregation. To show how H-adsorption affects segregation in nanoalloys, we compare the relative stability of configurations at x_{Pt} = 29/55, before and after H-adsorption at various sites and H-coverage in Figure 5. We note that Pt (Pd) prefers the core (shell) for the bare nanoalloy and H adsorbs more strongly to Pt at the bridge site (see Table 1) and may thus induce Pt segregation to the surface. For all configurations, the E_{ads} is calculated using (2)

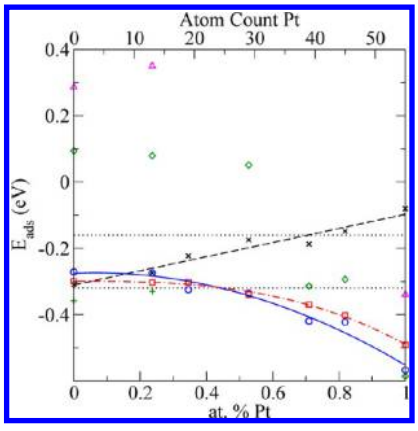

Figure 4. Mean E_{ads} of H on selected ground states for adsorption sites (see Figure 2), *a* (circle), *b* (square), *d* (+), *e* (cross), *g* (diamond), and *i* (triangle). Ground states include GS_{13}, GS_{19}, GS_{29}, GS_{39}, GS_{45}, pure Pd, and Pt. Best-fit curves are shown for sites *a*, *b*, and *e*. E_{ads} on bridge sites (*a* and *b*) follows a similar trend (strong at Pt but weak at Pd), as do atop sites (*g* and *i*). Hollow sites on {111} facets (*d* and *e*) show an opposite trend. E_{ads} bounded between horizontal dotted lines are predicted to be better HER catalysts than Pt (111) surface.[4]

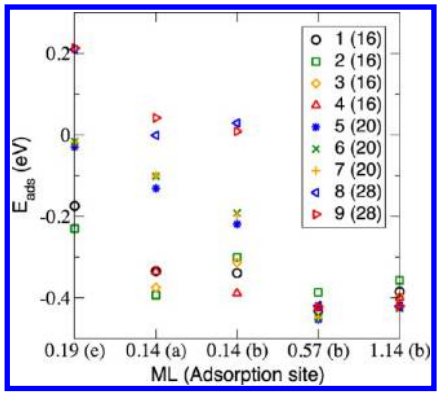

Figure 5. Mean E_{ads} of nine configurations at x_{Pt} = 29/55 (generated during the CE ground state search) for different ML of H at selected adsorption sites (see Figures 2 and S6 and S7). Configurations are ranked according to their stability (measured by E_f) before H-adsorption (GS_{29} is thus ranked 1 = most stable), and the number of surface Pt are in parentheses. The top four configurations have pure Pt cores but different atomic ordering on the shell.

with E_M being the energy of bare GS_{29}; hence E_{ads} measures the relative stability of configurations with adsorbed H. Figure 5 shows that, at low-H coverage, configurations with the same number of Pt (Pd) at the core (shell) have comparable stability (or E_{ads}). In contrast, configurations with more Pt in the shell could result in E_{ads} being 0.4 eV higher than that of the most stable case. Specific atomic arrangement on the shell affects stability to a lesser extent than if Pt atoms were segregated to the surface, which is also reflected in the CE (compare the single-point and multibody effective cluster interactions (ECI) in Table S1 of the Supporting Information). Thus low-coverage H-adsorption does not change the segregation behavior as the energy cost for Pt segregation to the shell is large. However, at high coverage (0.5 ML and beyond), E_{ads} are no longer sensitive to segregation; all energies are within 0.07 eV of one another. The energy cost to move Pt to the shell is now compensated by the stronger binding to Pt by a large number of H atoms at the bridge sites. Importantly, the E_{ads} of GS_{29} differs from the most stable case by at most 0.06 eV in all instances. Thus, errors incurred (using ground states of bare nanoalloy in adsorption calculations) are small enough not to alter the trend in Figure 4, which we can safely use to discuss the catalytic activity of HER below.

Effect on Hydrogen Evolution Reaction. To show how the adsorption trends would affect the catalysis of HER, $(1/2)H_2 \leftrightarrow H^* \leftrightarrow H^+ + e^-$, we utilize the model by Nørskov et al. which predicts the catalytic activity of HER electrodes via the adsorption free energies of H.[21,54,55] For transition-metal surfaces, the free energy of adsorption is approximately $\Delta G_{H^*} = E_{ads} + (0.04 + 0.20)$ eV (see the Supporting Information). Good HER electrocatalysts have values close to the optimal value of $\Delta G_{H^*} = 0$ or $E_{ads} = -0.24$ eV. Between the boundaries of $E_{ads} = -(0.24 \pm 0.08)$ eV in Figure 4, the adsorption site is expected to be more active than the hollow site of Pt (111) surface (our benchmark). Considering bridge sites and {111} hollow sites of Pt cuboctahedron, the adsorption at bridge (hollow) site is too strong (weak); Pt cuboctahedron is likely to be less catalytically active than Pt (111). Adding Pt, the H adsorption energies on the {111} and {100} facets are tuned continuously. At ca. 0.3 Pd, the H adsorption energy at {111} hollow site falls within the boundaries, and the activity of this facet is comparable to that of Pt (111). However, the bridge sites remain blocked by H atoms. A further increase in activity is expected beyond ca. 0.6 Pd, when the H adsorption energy at bridge sites also falls within the boundaries. Now both {111} and {100} facets are more active than Pt (111). The effective adsorption coverage considered for the NP are between 0.14 and 0.19 ML (see Figure S6), which are close to that of the surface at 0.25 ML. For more accurate predictions, adsorption energies at equilibrium H coverage are required.[53,56]

Conclusions. Using first-principles-based cluster expansion method together with simulated annealing, we conducted a comprehensive search for ground states of a 55-atom Pd–Pt cuboctahedral nanoalloy. The ground states exhibit Pt(core)–Pd(shell) structure across all compositions, agreeing with experimental findings. We calculated the hydrogen-adsorption properties of the ground states, showing that the energy trends versus Pd–Pt composition depend on adsorption site. In particular, adsorption energies on {111} hollow sites and {100} bridge sites exhibit opposing trends. We demonstrated the possibility of tuning NP catalyst behavior via alloying for the hydrogen-evolution reaction.

■ ASSOCIATED CONTENT

Ⓢ Supporting Information

Computational details, figures and table showing effective cluster interactions, comparison of predicted configurations with experiment, segregation on (100) surface, figures showing adsorption of multiple H atoms, and definition of adsorption free energy. This material is available free of charge via the Internet at http://pubs.acs.org.

■ AUTHOR INFORMATION

Corresponding Author

*E-mail: tantl@ihpc.a-star.edu.sg.

Notes

The authors declare no competing financial interest.

■ ACKNOWLEDGMENTS

T.L.T. acknowledges the use of supercomputers in A-STAR Computational Resource Centre (ACRC). T.L.T. and K.B.

acknowledge internal funding from Institute of High Performance Computing. T.L.T. initial support for CE Thermodynamic Tool Kit was from National Science Foundation (DMR-0705089). Work at Ames Laboratory was supported by the U.S. Department of Energy (DOE), Office of Science, Basic Energy Sciences (BES), Division of Materials Science and Engineering (Complex Hydrides). Ames Laboratory is operated for DOE by Iowa State University under Contract No. DE-AC02-07CH11358. Catalysis work was supported through Iowa State by DOE/BES Division of Chemical Science, Geosciences and Bioscience (DEFG02-03ER15476).

REFERENCES

(1) Ferrando, R.; Jellinek, J.; Johnston, R. L. *Chem. Rev.* **2008**, *108*, 845−910.
(2) Toshima, N.; Yonezawa, T. *New J. Chem.* **1998**, *22*, 1179−1201.
(3) Sanchez, S. I.; Small, M. W.; Zuo, J.; Nuzzo, R. G. *J. Am. Chem. Soc.* **2009**, *131*, 8683−8689.
(4) Wang, L.-L.; Johnson, D. D. *J. Am. Chem. Soc.* **2009**, *131*, 14023−14029.
(5) Lloyd, L. D.; Johnston, R. L.; Salhi, S.; Wilson, N. T. *J. Mater. Chem.* **2004**, *14*, 1691.
(6) Paz-Borbón, L. O.; Johnston, R. L.; Barcaro, G.; Fortunelli, A. *J. Phys. Chem. C* **2007**, *111*, 2936−2941.
(7) Rousset, J. L.; Khanra, B. C.; Cadrot, A. M.; Aires, F. J. C. S.; Renouprez, A. J.; Pellarin, M. *Surf. Sci.* **1996**, *352*−*354*, 583−587.
(8) Rousset, J. L.; Renouprez, A. J.; Cadrot, A. M. *Phys. Rev. B* **1998**, *58*, 2150−2156.
(9) Cheng, D.; Huang, S.; Wang, W. *Chem. Phys.* **2006**, *330*, 423−430.
(10) Barcaro, G.; Fortunelli, A.; Polak, M.; Rubinovich, L. *Nano Lett.* **2011**, *11*, 1766−1769.
(11) Sanchez, J. M.; Ducastelle, F.; Gratias, D. *Physica* **1984**, *128 A*, 334−350.
(12) Zarkevich, N. A.; Tan, T. L.; Wang, L.-L.; Johnson, D. D. *Phys. Rev. B* **2008**, *77*, 144208.
(13) Ducastelle, F.; Cyrot-Lackmann, F. *J. Phys. Chem. Solids* **1970**, *31*, 1295−1306.
(14) Ducastelle, F.; Cyrot-Lackmann, F. *J. Phys. Chem. Solids* **1971**, *32*, 285−301.
(15) Wang, L.-L.; Tan, T. L.; Johnson, D. D. *Phys. Rev. B* **2012**, *86*, 035438.
(16) Burch, R. *Acc. Chem. Res.* **1982**, *15*, 24−31.
(17) Maroun, F.; Ozanam, F.; Magnussen, O. M.; Behm, R. J. *Science* **2001**, *293*, 1811−1814.
(18) Tang, W.; Zhang, L.; Henkelman, G. *J. Phys. Chem. Lett.* **2011**, *2*, 1328−1331.
(19) Lu, C.-Y.; Henkelman, G. *J. Phys. Chem. Lett.* **2011**, *2*, 1237−1240.
(20) Marković, N. M.; Ross, P. N., Jr. *Surf. Sci. Rep.* **2002**, *45*, 117−229.
(21) Nørskov, J. K.; Bligaard, T.; Logadottir, A.; Kitchin, J. R.; Chen, J. G.; Pandelov, S.; Stimming, U. *J. Electrochem. Soc.* **2005**, *152*, J23−J26.
(22) Van Santen, R. A. *Acc. Chem. Res.* **2009**, *42*, 57−66.
(23) Yudanov, I. V.; Genest, A.; Schauermann, S.; Freund, H.-J.; Rösch, N. *Nano Lett.* **2012**, *12*, 2134−2139.
(24) Peng, Z.; Yang, H. *Nano Today* **2009**, *4*, 143−164.
(25) Aprà, E.; Baletto, F.; Ferrando, R.; Fortunelli, A. *Phys. Rev. Lett.* **2004**, *93*, 065502.
(26) Wang, L.-L.; Johnson, D. D. *J. Am. Chem. Soc.* **2007**, *129*, 3658−3664.
(27) Toshima, N.; Harada, M.; Yonezawa, T.; Kushihashi, K.; Asakura, K. *J. Phys. Chem.* **1991**, *95*, 7448−7453.
(28) Rousset, J. L.; Cadrot, A. M.; Cadete Santos Aires, F. J.; Renouprez, A.; Mélinon, P.; Perez, A.; Pellarin, M.; Vialle, J. L.; Broyer, M. *J. Chem. Phys.* **1995**, *102*, 8574−8585.
(29) Renouprez, A.; Rousset, J. L.; Cadrot, A. M.; Soldo, Y.; Stievano, L. *J. Alloys Compd.* **2001**, *328*, 50−56.
(30) Hohenberg, P.; Kohn, W. *Phys. Rev.* **1964**, *136*, B864−B871.
(31) Kohn, W.; Sham, L. J. *Phys. Rev.* **1965**, *140*, A1133−A1138.
(32) Kresse, G.; Furthmüller, J. *Comput. Mater. Sci.* **1996**, *6*, 15−50.
(33) Kresse, G.; Furthmüller, J. *Phys. Rev. B* **1996**, *54*, 11169−11186.
(34) Blöchl, P. E. *Phys. Rev. B* **1994**, *50*, 17953−17979.
(35) Perdew, J. P.; Wang, Y. *Phys. Rev. B* **1992**, *45*, 13244−13249.
(36) Hammer, B.; Hansen, L. B.; Nørskov, J. K. *Phys. Rev. B* **1999**, *59*, 7413−7421.
(37) Connolly, J. W. D.; Williams, A. R. *Phys. Rev. B* **1983**, *27*, 5169.
(38) Sluiter, M.; Turchi, P. *Phys. Rev. B* **1987**, *36*, 4630−4646.
(39) Ceder, G.; Garbulsky, G. D.; Avis, D.; Fukuda, K. *Phys. Rev. B* **1994**, *49*, 1−7.
(40) Wolverton, C.; Zunger, A.; Lu, Z.-W. *Phys. Rev. B* **1994**, *49*, 16058−61.
(41) Ozoliņš, V.; Wolverton, C.; Zunger, A. *Phys. Rev. B* **1998**, *58*, 5897−5900.
(42) Ozoliņš, V.; Wolverton, C.; Zunger, A. *Phys. Rev. B* **1998**, *57*, 6427.
(43) van de Walle, A.; Asta, M.; Ceder, G. *CALPHAD: Comput. Coupling Phase Diagrams Thermochem.* **2002**, *26*, 539−553.
(44) Asta, P.; Ozolins, V.; Woodward, C. *J. Org. Mater.* **2001**, *53*, 16−19.
(45) Zarkevich, N. A.; Johnson, D. D. *Phys. Rev. Lett.* **2004**, *92*, 255702.
(46) Hart, G. L. W.; Blum, V.; Walorski, M. J.; Zunger, A. *Nat. Mater.* **2005**, *4*, 391−394.
(47) Drautz, R.; Fahnle, M.; Sanchez, J. M. *J. Phys.: Condens. Matter* **2004**, *16*, 3834−3852.
(48) Drautz, R.; Díaz-Ortiz, A. *Phys. Rev. B* **2006**, *73*, 224207.
(49) Zarkevich, N. A.; Tan, T. L.; Johnson, D. D. *Phys. Rev. B* **2007**, *75*, 104203.
(50) Lerch, D.; Wieckhorst, O.; Hart, G. L. W.; Forcade, R. W.; Müller, S. *Modell. Simul. Mater. Sci. Eng.* **2009**, *17*, 055003.
(51) Mueller, T.; Ceder, G. *ACS Nano* **2010**, *4*, 5647−5656.
(52) Yuge, K. *J. Phys.: Condens. Matter* **2010**, *22*, 245401.
(53) Yang, F.; Zhang, Q.; Liu, Y.; Chen, S. *J. Phys. Chem. C* **2011**, *115*, 19311−19319.
(54) Schmickler, W.; Trasatti, S. *J. Electrochem. Soc.* **2006**, *153*, L31.
(55) Nørskov, J. K.; Bligaard, T.; Logadottir, A.; Kitchin, J. R.; Chen, J. G.; Pandelov, S.; Stimming, U. *J. Electrochem. Soc.* **2006**, *153*, L33.
(56) Skúlason, E.; Tripkovic, V.; Björketun, M. E.; Gudmundsdóttir, S.; Karlberg, G.; Rossmeisl, J.; Bligaard, T.; Jónsson, H.; Nørskov, J. K. *J. Phys. Chem. C* **2010**, *114*, 18182−18197.